Supplemental Material: Expansion dynamics of a shell-shaped Bose-Einstein condensate

Fan Jia,[1] Zerong Huang,[1] Liyuan Qiu,[1] Rongzi Zhou,[1] Yangqian Yan,[1,2] and Dajun Wang[1,2,*]

[1] *Department of Physics, The Chinese University of Hong Kong, Hong Kong SAR, China*
[2] *The Chinese University of Hong Kong Shenzhen Research Institute, Shenzhen, China*

(Dated: October 28, 2022)

SUPPLEMENTARY MATERIAL

Preparing the shell BEC in the magic wavelength trap

The double BEC is first created in an optical dipole trap formed by two crossing 1070 nm laser beams. Details of the evaporative cooling in this step have been discussed before [1, 2]. At this wavelength, the trap oscillation frequency of ^{23}Na atoms is about 10% higher than that of the ^{87}Rb atoms. The differential gravity sag is thus non-zero and the centers of mass of the two BECs are displaced from each other in the vertical direction. To overcome this issue, we load the double BEC adiabatically into the 946 nm magic wavelength crossed ODT in which the two BECs experience the same trap frequencies [3]. This is achieved by ramping off the 1070 nm light beams while ramping on two 946 nm beams in the same beam path. Figure S1A shows the external trap potentials without (top) and with (bottom) the gravitational effects in the magic wavelength trap. The gravity sag shifts the minima of the potentials downward by the same amounts. As the horizontal trap potential are not affected by gravity, the two BECs produced in this trap will share the same center of mass positions.

The final configuration for studying the shell BEC is reached after further evaporative cooling by lowering the power of the 946 nm light. At the end of this procedure, two condensates with typically 1.3×10^5 ^{23}Na atoms and 1.2×10^5 ^{87}Rb atoms without discernible thermal fractions are obtained routinely.

An intuitive way to understand the shape of the ^{23}Na shell is by looking at its effective trapping potential $V_1^{eff} = V_1 + U_{12}n_2$ as illustrated in Fig. S1B without (top) and with (bottom) gravity. Without gravity, the repulsive interspecies interaction divides V_1^{eff} in the vertical direction into two parts symmetrically. In this case, the ^{23}Na BEC will form a spherical shell. The distortion caused by gravity breaks this symmetry and leads to more atoms at the bottom. However, a closed shell can still form, unless the number of ^{87}Rb atoms is exceedingly large and the number of ^{23}Na is really small. This picture agrees well with results obtained from numerical calculations of the coupled GP equations shown in Fig.1 of the main text.

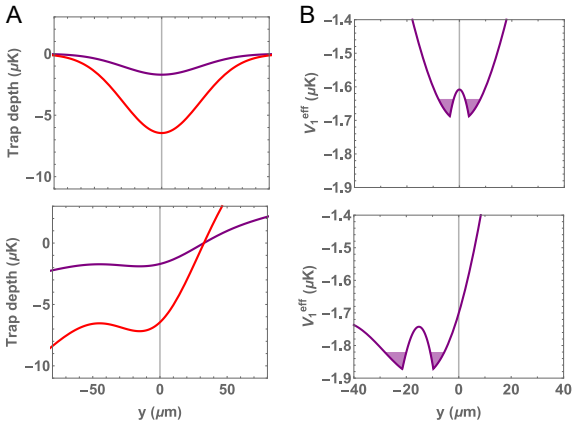

FIG. S1. The magic wavelength trap and the influence of gravity. (A) The calculated external trapping potentials generated by the 946 nm optical dipole trap for ^{23}Na and ^{87}Rb without (top) and with (bottom) gravity. The potentials are shifted and distorted by gravity. The distortion is especially severe for the shallower ^{23}Na potential. Nevertheless, the minima of the potentials are at the same position. (B) The effective trapping potential for ^{23}Na with contributions from the interspecies interaction without (top) and with (bottom) gravity. The shaded areas show schematically the ^{23}Na BEC filled in the shell-shaped trap for illustrating the origin of the asymmetric top and bottom atom distributions in the shell.

Probing the shell BEC

The relevant atomic levels for the ^{23}Na BEC detection are depicted in Fig. S2. As illustrated in Fig.1, to resolve the shell structure, we shape the optical pumping beam to a $15\mu m \times 800\mu m$ light sheet with cylindrical lenses. This allow us to cut out only a slice of the shell to be observed by absorption imaging with the probe beam.

The thickness of the slice can be reduced by using an optical pumping beam with large detuning, low power, and short pulse duration. However, due to the Gaussian beam profile, the minimum thickness is still more or less limited to the beam waist. As the result of this finite thickness and the curvature of the shell, the observed shell radius tends to be smaller than the real value. Ideally, to measure the shell size as accurate as possible, we should use the light sheet configuration which gives the thinnest slice. However, following the TOF expansion, the number of atoms can be optically pumped, and thus

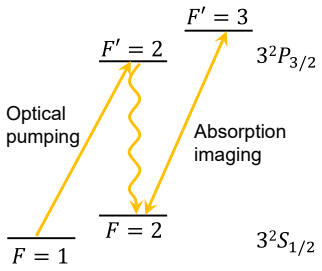

FIG. S2. Detection scheme of the ^{23}Na shell BEC. The atoms are first transferred from $F = 1$ to $F = 2$ via optical pumping before being detected with absorption imaging on the $F = 2 \rightarrow F' = 3$ cycling transition. The optical pumping beam has a thickness of 15 μm for resolving the structures of the expanded shell.

the signal, will be reduced. This is especially problematic for observing the interference fringes which already contain very small amounts of atoms.

With the understanding to these limitations, in the experiment, we adjust the optical pumping parameters empirically to achieve enough signal but at the same time minimize the thickness of the optically pumped slice of the shell.

Two imaging configurations are used in the experiment:

1) At very short total TOFs, the sizes of the BECs are only several microns and the inner radius of the ^{23}Na shell is smaller than the light sheet thickness. We use a 15× magnification imaging system with measured optical resolutions of 1.8 μm and 2.4 μm for ^{23}Na at 589 nm and ^{87}Rb at 780 nm, respectively. As the OD is high, to avoid strong attenuation of the optical pumping beam, its frequency is 160 MHz detuned from the $F = 1 \rightarrow F' = 2$ transition. This ensures all atoms in the light sheet are pumped to $F = 2$ with a uniform probability. A short pulse duration of 2 μs is used, and the power is varied from 0.07 mW to 3 mW. The data in Fig.2A and Fig.2B are obtained with this imaging configuration.

2) At longer TOFs, the size of the shell becomes too large for the 15× imaging system. To increase the field of view, we change to a 3× magnification imaging system with an estimated optical resolution of 4 μm. As the OD becomes lower following the expansion, attenuation of the optical pumping beam is not significant. The optical pumping light frequency is thus tuned to the $F = 1 \rightarrow F' = 2$ resonance to increase the signal. The optical pumping power and pulse duration are set to below 0.1 mW and 2 μs, respectively. The data in Fig.3A and Fig.4 are obtained with this configuration.

In Fig. S3, we show the absorption images of the ^{23}Na shell and the normal single species ^{23}Na BEC together. This proves that the fringes of the shell are not from defects of the detection process.

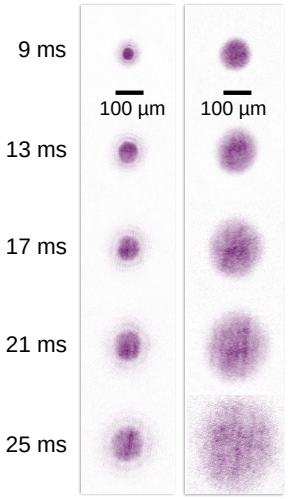

FIG. S3. Side by side comparison of the absorption images of the ^{23}Na shell (left) and the single species ^{23}Na BEC (right). During the expansion, no patterns are observed for the single species BEC.

Numerical simulation

The in-trap density of ^{23}Na in Fig.1B and the release energies in Fig.2D are obtained by solving the coupled GPEs numerically. The external potential V_i includes contributions from both the ODT and gravity. The Gaussian-shaped ODT trap can be well approximated by a harmonic function near its center. However, the gravity magnifies the anharmonicity, and distorts the potential. In the simulation, we represent V_i with a polynomial up to the 4th order

$$V_i = \frac{m_i}{2}(\omega_x^2 x^2 + \omega_z^2 z^2) + \frac{m_i}{2}\omega_y^2 (y + \Delta y)^2 + \beta(y + \Delta y)^3 + \gamma(y + \Delta y)^4, \tag{S1}$$

where the ratio $\beta/(m_i\omega_y^2/2) \sim 0.06$ and $\gamma/(m_i\omega_y^2/2) \sim 0.001$ are obtained from fitting to the calculated full trapping potential based on measured trap frequencies and beam waists.

Limited by the thickness resolution of the light sheet, the expansion dynamics of the hollow shell in very short time scales cannot be measured in the experiment. Figure S4 shows the dynamics in this period from numeri-

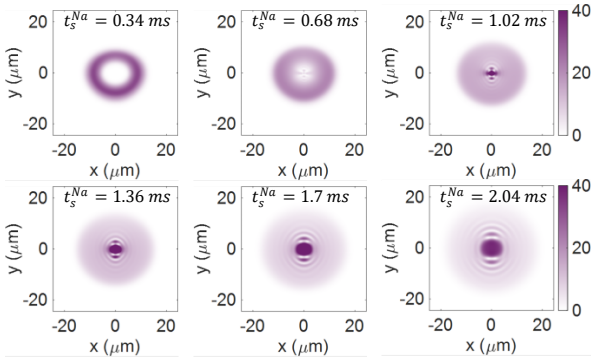

FIG. S4. Short time expansion dynamics of the hollow shell from numerical simulation. The shell is created after $t_{co} = 0.34$ ms. The implosion happens faster in the vertical direction due to the higher trap frequency. This also results in higher fringe contrast in the vertical direction. At 2.04 ms, the main features of the self-interference already match with those observed in the experiment. The increase in the outer size indicates explosion occurs simultaneously with implosion. The unit in the color bar is μm^{-3}.

cal simulation for the hollow shell created after 0.34 ms co-expansion. In the first 2 ms, both implosion and explosion will happen. The self-interference fringes become visible once the atoms reach the center following the implosion at around 1 ms. Afterwards, both the number of atoms accumulated at the center and the fringe spacings increase with TOF. Importantly, due to the higher trap frequency in the vertical direction, the fringes in the x and y directions are not identical. In the vertical direction, the visibility is always higher. This is why we choose this part of the image in the data processing. The patterns at $t_s^{\rm Na} = 2.04$ ms are already similar to the experimentally observed ones for longer $t_s^{\rm Na}$.

Release energy measurement

Traditionally, the release energy is defined for a BEC released from a trap as $E_{\rm rel} = E_{\rm k} + E_{\rm int}$, with $E_{\rm k}$ the quantum pressure and $E_{\rm int}$ the interaction energy [4–6]. At longer TOFs, all energy will be converted into the kinetic energy of the expansion. The $E_{\rm rel}$ in Fig. 2C and Fig. 2D are defined in the same way but for ^{87}Rb BECs released from the ^{23}Na shell after a range of co-expansion time $t_{\rm co}$, instead of from the optical trap. This allows us to observe the energy transfer between the inner BEC and the shell during their co-expansion.

Experimentally, $E_{\rm rel}$ after each $t_{\rm co}$ is measured by first removing the ^{23}Na shell, and then taking the absorption image of the ^{87}Rb BEC after it expands alone for a certain $t_s^{\rm Rb}$. The zero point of $t_s^{\rm Rb}$ is at the moment of the ^{23}Na shell removal. The rms radii $\sigma(t_s^{\rm Rb})$ of the ^{87}Rb BEC are extracted from the 2D parabolic fitting following the Thomas-Fermi approximation. $E_{\rm rel}$ can then be calculated from the expansion velocity v of the sample obtained by fitting to $\sigma(t_s^{\rm Rb}) = \sqrt{\sigma_0^2 + (v\ t_s^{\rm Rb})^2}$, with σ_0 the initial size of the sample. We note that the $E_{\rm rel}$ presented in Fig. 2C and Fig. 2D include contributions from all three directions. We assumed cylindrical symmetry in order to get the release energy along the imaging direction.

Image processing and data analysis

Due to the reduced number density, the signal of the shell decrease following the TOF expansion. For total TOF longer than 10 ms, the background noise, mainly because of light interference, becomes apparent. To increase the signal to noise ratio, we apply a fast Fourier transformation to the original OD image and mask out the high frequency noises. An OD image with improved quality is then obtained with an inverse fast Fourier transformation.

To extract more detailed information of the shell and the interference fringes, we first convert the OD image from Cartesian coordinates to polar coordinates. For the expansion of the filled shell, the size is obtained from a Gaussian fitting to the azimuthally averaged 1D profile between polar angles 170° to 190°. The azimuthal average does not include the full 360° data as the image is not perfectly spherical. For the expansion of the hollow shell, to find the spacing between the self-interference fringes, we fit the data near each peak with a Gaussian to obtain the center of the peak. The fringe spacing is then the distance between the first and the second fringes.

* djwang@cuhk.edu.hk

[1] F. Wang, D. Xiong, X. Li, D. Wang, and E. Tiemann, Observation of Feshbach resonances between ultracold Na and Rb atoms, Phys. Rev. A **87**, 1 (2013).
[2] F. Wang, X. Li, D. Xiong, and D. Wang, A double species ^{23}Na and ^{87}Rb Bose-Einstein condensate with tunable miscibility via an interspecies Feshbach resonance, J. Phys. B **49**, 015302 (2015).
[3] M. S. Safronova, B. Arora, and C. W. Clark, Frequency-dependent polarizabilities of alkali-metal atoms from ultraviolet through infrared spectral regions, Phys. Rev. A **73**, 1 (2006).
[4] M.-O. Mewes, M. R. Andrews, N. J. van Druten, D. M. Kurn, D. S. Durfee, and W. Ketterle, Bose-Einstein condensation in a tightly confining dc magnetic trap, Phys. Rev. Lett. **77**, 416 (1996).
[5] M. J. Holland, D. S. Jin, M. L. Chiofalo, and J. Cooper, Emergence of interaction effects in Bose-Einstein condensation, Phys. Rev. Lett. **78**, 3801 (1997).
[6] Z. Guo, F. Jia, L. Li, Y. Ma, J. M. Hutson, X. Cui, and D. Wang, Lee-Huang-Yang effects in the ultracold mixture

of ^{23}Na and ^{87}Rb with attractive interspecies interactions,
Phys. Rev. Research **3**, 1 (2021).